

Identifying mechanisms in the control of quantum dynamics through Hamiltonian encodingAbhra Mitra^{1,*} and Herschel Rabitz²¹*Department of Electrical Engineering, Princeton University, Princeton, New Jersey 08544*²*Department of Chemistry, Princeton University, Princeton, New Jersey 08544*

(Received 1 July 2002; published 26 March 2003)

A variety of means are now available to design control fields for manipulating the evolution of quantum systems. However, the underlying physical mechanisms often remain obscure, especially in the cases of strong fields and high quantum state congestion. This paper proposes a method to quantitatively determine the various pathways taken by a quantum system in going from the initial state to the final target. The mechanism is revealed by encoding a signal in the system Hamiltonian and decoding the resultant nonlinear distortion of the signal in the system time-evolution operator. The relevant interfering pathways determined by this analysis give insight into the physical mechanisms operative during the evolution of the quantum system. A hierarchy of mechanism identification algorithms with increasing ability to extract more detailed pathway information is presented. The mechanism identification concept is presented in the context of analyzing computer simulations of controlled dynamics. As illustrations of the concept, mechanisms are identified in the control of several simple, discrete-state quantum systems. The mechanism analysis tools reveal the roles of multiple interacting quantum pathways to maximally take advantage of constructive and destructive interference. Similar procedures may be applied directly in the laboratory to identify control mechanisms without resort to computer modeling, although this extension is not addressed in this paper.

DOI: 10.1103/PhysRevA.67.033407

PACS number(s): 32.80.Qk

I. INTRODUCTION

Optimal control theory is an effective technique for designing electric fields to manipulate the evolution of quantum-mechanical systems [1–6]. Closed-loop learning algorithms [2] combined with advances in laser pulse-shaping techniques have enabled the direct discovery of laboratory optimal controls, even for complex systems [7–14]. However, the mechanisms by which the target state is reached often remain obscure, in both computer simulations and experiments. Under favorable conditions information about the control mechanism may be deduced from an analysis of the temporal, frequency, or time-frequency structure of the control fields [15,16]. However, under general circumstances caution is called for as the mechanism can depend in a nonlinear fashion on the control field. Thus, a more systematic technique is required, which addresses the nonlinearities of the mechanism identification problem. This paper presents the means to understand the control mechanism in the theoretical design of fields and their simulated dynamic response. The control mechanism is revealed by identifying the dominant quantum pathways contributing to the observable final state achieved by the control field. The pathways, and thus the system mechanism, can be resolved at various levels of detail. The notion of a quantum pathway is also subject to the definition associated with the choice of representation of the Hamiltonian, and this paper uses a natural definition in the context of applications described by a discrete set of states. However, some systems might lend themselves to other definitions of mechanism, which may be similarly revealed.

The mechanism identification concept

The essence of the mechanism identification (MI) concept will be explained below with the remainder of the paper presenting the details of the procedure and its illustration on several simple problems. A quantum control pathway analysis can be used for post-field-design MI as well as during the design procedure, to actively steer the dynamics to favor certain pathways. Analogous MI pathway analyses could be performed directly in the laboratory [17]. This paper concentrates on introducing the MI concept in the context of analysis after computational control field design. The basic procedure for MI remains the same when working with laboratory data, but additional complexities must be dealt with as direct access to the wave function is not available.

The quantum systems analyzed in this paper are described by Hamiltonians of the form $H = H_0 + V(t)$, where H_0 is the field-free Hamiltonian and $V(t)$ accounts for the external field. For many quantum control applications typically $V(t) = -\mu\mathcal{E}(t)$ where μ is the dipole and $\mathcal{E}(t)$ is the control electric field. Although the paper will assume this form for $V(t)$, the general formulation of Hamiltonian encoding does not require the Hamiltonian to be linear in the control field. The time evolution of the system is prescribed by the equation

$$i\hbar \frac{dU(t)}{dt} = [H_0 - \mu\mathcal{E}(t)]U(t), \quad U(0) = 1. \quad (1)$$

The eigenvalues E_i and eigenfunctions $|n_i\rangle$ of H_0 satisfy $H_0|n_i\rangle = E_i|n_i\rangle$ for $i = 1, 2, \dots, d$ where d is the dimension of the state space of the quantum system. We define $\omega_{ij} = (E_i - E_j)/\hbar$, and the control field can be conveniently expressed as

*Electronic address: abhra@princeton.edu

$$\mathcal{E}(t) = A(t) \sum_{i=1}^d \sum_{j<i} a_{ij} \sin(\omega_{ij}t + \phi_{ij}), \quad (2)$$

where $A(t)$ is a slowly varying envelope function. The actual control variables are the phases $\{\phi_{ij}\}$ and amplitudes $\{a_{ij}\}$. Making the transformation $V_I(t) = -\exp(iH_0t/\hbar)\mu\mathcal{E}(t)\exp(-iH_0t/\hbar)$ gives

$$i\hbar \frac{dU(t)}{dt} = V_I(t)U(t), \quad (3)$$

where U is now understood to be in the interaction representation. The solution of Eq. (3) is the matrix $U(T)$ with a basic focus of MI being an understanding of how a particular (often high) amplitude $U_{ba}(T)$ is achieved in state $|b\rangle$ at time T by the action of $\mathcal{E}(t)$ starting in state $|a\rangle$ at time $t=0$. Although knowledge of the matrix $U(T)$ prescribes all possible system observables at time T , the calculation of $U(T)$ does not generally reveal how the evolution occurs (i.e., the mechanism). The proposed MI algorithm can be understood by viewing the quantum system as a functioning ‘‘machine’’ under dynamical evolution, driven by the Hamiltonian $H(t) = H_0 - \mu\mathcal{E}(t)$. This situation is analogous to considering any functioning machine where an understanding of its operating mechanism is usually best achieved by applying external disturbances (e.g., perturbations) and monitoring the resultant transient system responses. If the disturbances are introduced in a suitable fashion, then the resultant response data can yield detailed information about the inner ‘‘workings’’ of the functioning machine. This logic applies equally well to quantum-dynamical machines.

Before considering how to modulate the quantum dynamics for MI, it is first necessary to define what we mean by ‘‘mechanism.’’ In the context of analyzing the mechanism for achieving the particular amplitude $U_{ba}(T)$ it is natural to seek out the important pathways leading from $|a\rangle$ to $|b\rangle$. Here a pathway is specified by a sequence of transitions $|a\rangle \rightarrow |l_1\rangle \rightarrow |l_2\rangle \rightarrow \dots \rightarrow |l_{n-1}\rangle \rightarrow |b\rangle$ where the states $|l_i\rangle$, $i=1, 2, \dots, n-1$, prescribe one particular path of n steps from $|a\rangle$ to $|b\rangle$. Such a path will have an associated amplitude denoted by $U_{ba}^{n(l_1, \dots, l_{n-1})}$. The total amplitude $U_{ba}(T)$ is then the sum of all contributing pathway amplitudes

$$U_{ba}(T) = \sum_{n, \{l_i\}} U_{ba}^{n(l_1, \dots, l_{n-1})}(T). \quad (4)$$

As a notational shorthand we may simply denote the set of amplitudes as $U_{ba}^n(T) \equiv U_{ba}^{n(l_1, \dots, l_{n-1})}$ where the intermediate states are implicitly understood. Figure 1(a) shows a schematic of the pathways leading from $|a\rangle$ to $|b\rangle$ labeled by the corresponding amplitudes.

The decomposition of $U_{ba}(T)$ in Eq. (4) is fully consistent with the general notion of quantum control operating by constructive interference between the amplitudes for all significant pathways leading from the initial state $|a\rangle$ to the final state $|b\rangle$. The present paper will present an efficient algorithm for determining the set of all relevant pathway amplitudes $\{U_{ba}^{n(l_1, \dots, l_{n-1})}\}$ connecting $|a\rangle$ and $|b\rangle$, whereby an analysis of

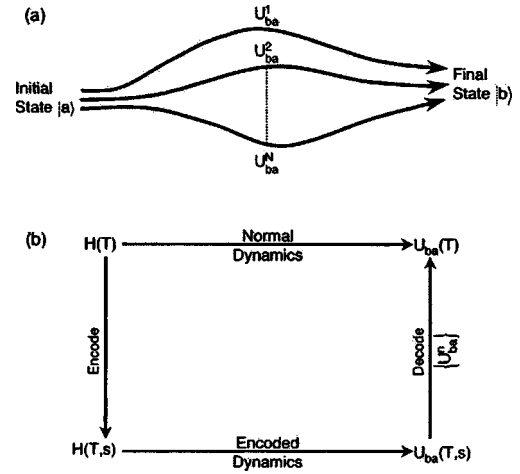


FIG. 1. A schematic showing the basic concept of pathway identification by Hamiltonian encoding. (a) A matrix element of the time-evolution operator $U_{ba}(T)$ can be decomposed into a set of $n=1, 2, \dots, N$ significant pathways $\{U_{ba}^n\}$ which constructively and destructively interfere to make effective the transition $|a\rangle \rightarrow |b\rangle$ under the action of the Hamiltonian $H(t)$, $0 \leq t \leq T$. If the population in $|b\rangle$ is significant (insignificant) then the pathways add up constructively (destructively) to give a net transfer of population. The mechanism is revealed by the magnitude and phases of the N pathway amplitudes $\{U_{ba}^n\}$. (b) The pathways are identified in a three-step process of (i) encoding the Hamiltonian features in terms of a characteristic variable s , which is scanned, (ii) performance of encoded dynamics to yield $U(T,s)$, and (iii) decoding of $U(T,s)$ through an inverse transform over the variable s to obtain $\{U_{ba}^n\}$, which reveals the dynamical mechanism of the original, uncoded system undergoing normal dynamics.

the set provides a means to understand the mechanism in computational quantum dynamics.

The amplitudes defining the mechanism of the controlled evolution may be directly associated with the terms contained in the Dyson expansion for the time evolution operator in the interaction picture [18] (while the term pathway invites comparison to Feynmann paths, these control pathways do not correspond to Feynmann paths [19])

$$U(T) = I + \left(\frac{-i}{\hbar}\right) \int_0^T V_I(t_1) dt_1 + \left(\frac{-i}{\hbar}\right)^2 \int_0^T V_I(t_2) \int_0^{t_2} V_I(t_1) dt_1 dt_2 + \dots \quad (5)$$

Here I is the $d \times d$ identity matrix. The next term is of order $n=1$, while the highest term explicitly shown in Eq. (5) is of order $n=2$, etc. The n th-order term in the expansion is the sum of all n th-order pathways prescribed by all possible intermediate steps $\{l_i\}$, $i=1, \dots, n-1$. Here the notion of order n is exactly coincident with its use in $U_{ba}^{n(l_1, \dots, l_{n-1})}(T)$ defined above. In order to determine the mechanistic information contained in Eq. (5), the physically relevant integrals need to be determined. The important integrals are those of significant magnitude connecting states $|a\rangle$ and $|b\rangle$, and a MI analysis must deal with an *a priori* lack of knowledge about

which integrals to focus on. A direct numerical approach to evaluating these multiple integrals would be exceedingly difficult, especially with strong fields where integrals (pathways) of high order may contribute significantly to $U(T)$. The MI technique introduced in this paper avoids this problem by *encoding* a signal into the Hamiltonian and *decoding* its effect on the output of the resultant distorted time evolution operator. This procedure provides a practical means for MI by computing all relevant terms in Eq. (5) in a simple fashion without explicit evaluation of the integrals.

The concept of encoding the Hamiltonian with a special signal and monitoring the observable response is a particular incarnation of the general procedure of introducing a disturbance in the dynamics in order to understand the dynamical mechanism. The encoding technique may be viewed as a modulation of the Hamiltonian by an input signal with the goal of attaining MI from the effect of the signal upon $U_{ba}(T)$. Normally, modulation for this purpose would be introduced as a function of time t outside the frequency range appearing in the quantum dynamics and the control field. In this way the modulating signal would act as a tracer, distinguished from the effects of the control field, so as to reveal the control mechanism from the distortions of the tracer signal appearing in the observations. However, the introduction of modulation frequencies in the tracer much higher than that of the natural dynamics would have a number of undesirable features. First, integrating the Schrödinger equation with a much finer time mesh than normal would be required, resulting in corresponding additional computational costs. Secondly, looking ahead to the laboratory implementation of MI such high-frequency input-modulation signals, even if they could be generated, would likely excite unwanted dynamics (e.g., electronic excitations). An alternative encoding technique is available for computational MI, introduced in this paper, which is also extendable to a form amenable for laboratory implementation.

As an illustration of the encoding technique consider the case of dipole coupling in the Hamiltonian such that each linkage in the sequence $|a\rangle \rightarrow |l_1\rangle \rightarrow |l_2\rangle \rightarrow \dots \rightarrow |l_{n-1}\rangle \rightarrow |b\rangle$ is given by a particular matrix element μ_{ij} , where i and j are members of the set $\{|a\rangle, |b\rangle, |l_i\rangle, i=1, \dots, n-1\}$. For encoding we may then modify the Hamiltonian matrix element $H_{ij} = E_i \delta_{ij} - \mu_{ij} \mathcal{E}(t)$ to become $H_{ij} = E_i \delta_{ij} - m_{ij}(s) \mu_{ij} \mathcal{E}(t)$, where $m_{ij}(s)$ is a suitably chosen encoding function of the variable s for $-\infty < s < \infty$. The resultant dynamics under the new Hamiltonian $H(s)$ will accordingly produce an altered transition matrix $U(T, s)$ which is a function of s . The goal is to choose $m_{ij}(s)$ such that each dipole element in the Hamiltonian produces a unique feature in $U(T, s)$ as the variable s is scanned. Furthermore, it is required that the deconvolution of $U(T, s)$ over the variable s yield all of the relevant amplitudes $U_{ba}^{n(l_1, \dots, l_{n-1})}(T)$. One possible approach is to modulate with Fourier functions $m_{ij}(s) \sim \exp(i\gamma_{ij}s)$ and deconvolute $U_{ba}(T, s)$ by a Fourier transform,

$$\tilde{U}_{ba}(T, \gamma) = \int_{-\infty}^{\infty} U_{ba}(T, s) e^{-i\gamma s} ds. \quad (6)$$

In this case the frequencies $\{\gamma_{ij}\}$ would be chosen to ensure

a unique encoding for $\{\mu_{ij}\}$, and then the amplitudes of the fundamental and combination spectral lines of $\tilde{U}_{ba}(T, \gamma)$ as a function of γ can be used to directly determine the desired amplitudes $U_{ba}^{n(l_1, \dots, l_{n-1})}$. Importantly, the modulation is introduced with respect to the variable (parameter) s , so the time dependence of the dynamics continues to have normal behavior. In practice this encoding/decoding operation would be implemented by repeatedly solving the Schrödinger equation at a sufficient set of discrete values for s such that the relevant spectrum $\tilde{U}_{ba}(T, \gamma)$ is fully covered in γ . This concept is schematically illustrated in Fig. 1(b). The techniques employed here are related to various nonlinear sensitivity analysis procedures [20,21], but the latter methods are generally confined to exploring the impact of system uncertainties.

The synopsis of the Hamiltonian encoding/decoding MI technique presented above is fully developed and illustrated in the remainder of the paper. Section II of the paper gives a precise definition of a quantum control pathway and Sec. III presents the concept of Hamiltonian encoding. Section IV considers a hierarchy of encoding techniques and pathway analyses to reveal different levels of detail about the mechanism. Some numerical examples are given in Sec. V and concluding remarks are given in Sec. VI.

II. QUANTUM CONTROL PATHWAYS

Consider a quantum-mechanical system in the interaction picture evolving under the Schrödinger equation (3). The system is initially in state $|a\rangle$ and the control goal is to take the system to the target state $|b\rangle$ at time T . These two states are members of a complete orthonormal set $|1\rangle, |2\rangle, \dots, |d\rangle$ of dimension d , which describes the subspace containing all the system dynamics. These states may arise in many ways depending upon the physical situation (i.e., they may be eigenstates of H_0 or some other physically motivated operator of the system). The MI objective is to discern all relevant pathways connecting $|a\rangle$ and $|b\rangle$ during the evolution of the system, as indicated in Fig. 1. Expressing Eq. (5) in the explicit basis, assuming $|b\rangle \neq |a\rangle$, using the notation $v_{mn}(t) = (-i/\hbar) \langle m | V_I(t) | n \rangle$ and $U_{ba} = \langle b | U(T) | a \rangle$,

$$\begin{aligned} U_{ba} = & \int_0^T v_{ba}(t_1) dt_1 + \sum_{l=1}^d \int_0^T v_{bl}(t_2) \int_0^{t_2} v_{la}(t_1) dt_1 dt_2 \\ & + \sum_{j=1}^d \sum_{k=1}^d \int_0^T v_{bj}(t_3) \int_0^{t_3} v_{jk}(t_2) \int_0^{t_2} v_{ka}(t_1) dt_1 dt_2 dt_3 \\ & + \dots \end{aligned} \quad (7)$$

A particular pathway is specified by the sequence of states starting from the initial state $|a\rangle$ and ending at the final state $|b\rangle$. The n th-order pathway with $n-1$ intermediate states, l_1, l_2, \dots, l_{n-1} will be denoted as $(a \rightarrow l_1 \rightarrow l_2 \rightarrow \dots \rightarrow l_{n-1} \rightarrow b)$, and will have a corresponding transition amplitude given by

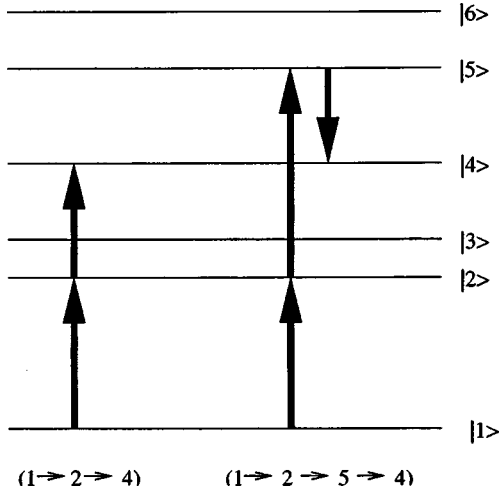


FIG. 2. An illustration of two possible paths from state $|1\rangle$ to $|4\rangle$ in a six-level system with corresponding amplitudes $U_{41}^{2(2)}$ and $U_{41}^{3(2,5)}$.

$$\begin{aligned}
 U_{ba}^{n(l_1, \dots, l_{n-1})} &= \int_0^T \int_0^{t_n} \dots \int_0^{t_2} v_{b l_{n-1}}(t_n) v_{l_{n-1} l_{n-2}}(t_{n-1}) \dots \\
 &\quad \times v_{l_1 a}(t_1) dt_1 \dots dt_{n-1} dt_n. \tag{8}
 \end{aligned}$$

The transition amplitude associated with a pathway is the contribution it makes to the evolution of the system. The value of U_{ba} will be given by the sum of the transition amplitudes along all possible pathways starting at $|a\rangle$ and ending at $|b\rangle$. Therefore

$$U_{ba} = \sum_{n=1}^{\infty} \sum_{l_1, \dots, l_{n-1}=1}^d U_{ba}^{n(l_1, \dots, l_{n-1})}. \tag{9}$$

A pathway is considered to be significant if the absolute value of its transition amplitude $|U_{ba}^{n(l_1, \dots, l_{n-1})}|$ is large compared to the transition amplitudes of other pathways or greater than some specified minimum value.

As an example, consider a six-level system where the transition of interest is from state $|1\rangle$ to $|4\rangle$. Then the amplitude of the second-order pathway corresponding to this transition occurring via the state $|2\rangle$ is given by

$$U_{41}^{2(2)} = \int_0^T \int_0^{t_2} v_{42}(t_2) v_{21}(t_1) dt_1 dt_2.$$

Similarly the transition amplitude for the third-order pathway $(1 \rightarrow 2 \rightarrow 5 \rightarrow 4)$ would be

$$U_{41}^{3(2,5)} = \int_0^T \int_0^{t_3} \int_0^{t_2} v_{45}(t_3) v_{52}(t_2) v_{21}(t_1) dt_1 dt_2 dt_3.$$

Both of these pathways are illustrated in Fig. 2.

Knowledge of the set of dominant pathways contributing to the evolution of the system reveals the control mechanism. If the states $\{|e\rangle\}$ are identified as eigenstates of H_0 , and if a

certain path $(a \rightarrow l_1 \rightarrow l_2 \rightarrow \dots \rightarrow l_{n-1} \rightarrow b)$ has a significant transition amplitude, then this contribution to the mechanism involves the corresponding sequence of n stimulated absorption/emission processes. In the commonly expected situation where multiple pathways with transition amplitudes $U_{ba}^{n(l_1, \dots, l_{n-1})}$, $U_{ba}^{n'(l'_1, \dots, l'_{n-1})}$, etc., all contribute significantly to the transition $|a\rangle \rightarrow |b\rangle$, an important issue is the degree of constructive interference among these pathways [7,22]. Each amplitude is a complex number with an associated phase $\phi_{ba}^{n(l_1, \dots, l_{n-1})}$. If the various phases are nearly equal ($\phi_{ba}^{n(l_1, \dots, l_{n-1})} \approx \phi_{ba}^{n'(l'_1, \dots, l'_{n-1})} \dots$), then the amplitudes will add up constructively at the final time implying an efficient control process in steering the system from $|a\rangle$ to $|b\rangle$. The pathway analyses of systems in this paper driven by optimal fields showed excellent alignment of pathway phases for constructive interference in the target state. A good optimal control solution for population transfer from $|a\rangle$ to $|b\rangle$ will yield $|U_{ba}(T)| \approx 1$ and $|U_{ca}(T)| \approx 0$ for $c \neq b$. In the latter case a pathway analysis is expected to show that the multiple amplitudes contributing to $U_{ca}(T)$ destructively interfere with each other to produce the nearly zero net amplitude.

III. HAMILTONIAN ENCODING

Prior to the performance of MI, a control field would be prescribed by some appropriate means (e.g., optimal control theory [1,6,23]). The identification of the relevant pathways and their transition amplitudes $U_{ba}^{n(l_1, \dots, l_{n-1})}$ is the central step in revealing the underlying quantum control mechanisms. As stated in Sec. I a direct computation of the integrals defining the pathway amplitudes can, in principle, be done. However, it is a forbidding task, especially for high-order pathways. The Hamiltonian encoding procedure bypasses this problem by modulating the Hamiltonian in a special manner and deducing the pathway amplitudes by decoding the nonlinear system response to this modulation in the output U_{ba} .

The technique operates with just the ability to numerically solve Schrödinger's equation. In general, encoding the Hamiltonian is done by modulating the matrix elements of the interaction term V_I such that each pathway amplitude $U_{ba}^{n(l_1, \dots, l_{n-1})}$ has a unique signature in U_{ba} which can then be read off at the end of the computation. Different encoding schemes can be employed for this purpose to provide distinct levels of detail about the mechanism.

An examination of Eq. (7) indicates that any modulation in the time variable would distort each pathway in a very complex fashion, making recovery of the original transition amplitudes of Eqs. (8) and (9) very difficult. This problem may be circumvented by introducing a timelike variable s and modulating the system in this variable. Multiple timelike variables s_1, s_2, \dots may also be introduced to some benefit in certain cases, but this extension will not be treated here.

The most general modulation scheme (in one variable s) for the coupling elements is

$$v_{ij}(t) \rightarrow v_{ij}(t) m_{ij}(s).$$

The original Schrödinger equation with the coupling matrix explicitly shown is

$$\frac{dU(t)}{dt} = \begin{pmatrix} v_{11}(t) & v_{12}(t) & \cdots & v_{1d}(t) \\ v_{21}(t) & v_{22}(t) & \cdots & v_{2d}(t) \\ \cdot & \cdot & \cdot & \cdot \\ \cdot & \cdot & \cdot & \cdot \\ v_{d1}(t) & v_{d2}(t) & \cdots & v_{dd}(t) \end{pmatrix} U(t), \quad (10)$$

which now becomes

$$\frac{dU(t,s)}{dt} = \begin{pmatrix} v_{11}(t)m_{11}(s) & v_{22}(t)m_{12}(s) & \cdots & v_{1d}(t)m_{1d}(s) \\ v_{21}(t)m_{21}(s) & v_{22}(t)m_{22}(s) & \cdots & v_{2d}(t)m_{2d}(s) \\ \cdot & \cdot & \cdot & \cdot \\ \cdot & \cdot & \cdot & \cdot \\ v_{d1}(t)m_{d1}(s) & v_{d2}(t)m_{d2}(s) & \cdots & v_{dd}(t)m_{dd}(s) \end{pmatrix} U(t,s). \quad (11)$$

In the integration of Eq. (11) over time the variable s is a constant, implying that the transition amplitude for the path ($a \rightarrow l_1 \rightarrow \cdots \rightarrow l_{n-1} \rightarrow b$) becomes

$$\begin{aligned} U_{ba}^{n(l_1, \dots, l_{n-1})}(s) &= \int_0^T \cdots \int_0^{t_n} v_{bl_{n-1}}(t_n) m_{bl_{n-1}}(s) \cdots v_{l_1 a}(t_1) \\ &\quad \times m_{l_1 a}(s) dt_1 \cdots dt_n \\ &= U_{ba}^{n(l_1, l_2, \dots, l_{n-1})} M_{ba}^{n(l_1, l_2, \dots, l_{n-1})}(s), \end{aligned} \quad (12)$$

$$M_{ba}^{n(l_1, l_2, \dots, l_{n-1})}(s) = m_{bl_{n-1}}(s) m_{l_{n-1} l_{n-2}}(s) \cdots m_{l_1 a}(s). \quad (13)$$

Here $M_{ba}^{n(l_1, \dots, l_{n-1})}(s)$ is the characteristic function associated with the particular pathway ($a \rightarrow l_1, \dots, l_{n-1} \rightarrow b$). The encoding functions $m_{ij}(s)$ are chosen such that each path will be modulated in a unique way as a function of s . By solving the Schrödinger equation at a suitable set of s values, the amplitudes of the relevant paths can be extracted from a decoding of $U_{ba}(s) \equiv \langle b | U(T, s) | a \rangle$. Then, from Eqs. (8)–(12), the overall amplitude $U_{ba}(s)$ for the system evolving from the state $|a\rangle$ to $|b\rangle$ over the time interval $0 \leq t \leq T$ becomes

$$\begin{aligned} U_{ba}(s) &= \sum_{n=1}^{\infty} \sum_{l_1, l_2, \dots, l_{n-1}=1}^d U_{ba}^{n(l_1, l_2, \dots, l_{n-1})} \\ &\quad \times M_{ba}^{n(l_1, l_2, \dots, l_{n-1})}(s). \end{aligned} \quad (14)$$

The utility of introducing modulation through the variable s lies in the form of Eq. (14) upon comparison to Eq. (9). Time-domain modulation would completely distort the tran-

sition amplitude of each path, i.e., $U_{ba}^{n(l_1, \dots, l_{n-1})}$ would have changed in an undecipherable way. Modulation in terms of the extra variable s will also (possibly severely) distort the total time-evolution operator $U_{ba}(s)$. However, the distortion has, by construction, a very special form which is conveniently expressed in terms of the original undistorted amplitudes for each individual pathway $U_{ba}^{n(l_1, \dots, l_{n-1})}$, multiplied by a known function $M_{ba}^{n(l_1, \dots, l_{n-1})}(s)$. This formulation provides considerable freedom in the choice of $m_{ij}(s)$ as the amplitudes $U_{ba}^{n(l_1, \dots, l_{n-1})}$ in Eq. (14) remain unchanged even with the most violent s -domain modulation. Equation (14) is exact for any form of s -domain modulation, regardless of the form of $m_{ij}(s)$. Provided that the $\{m_{ij}\}$ are bounded in magnitude, the expansion in Eq. (14) will always converge as discussed in the Appendix. The MI analysis in Sec. IV will exploit this encoding flexibility by even making the system matrix $\{v_{ij}(t)m_{ij}(s)\}$ non-Hermitian in order to distinguish between certain quantum pathways. Another scheme for extracting very fine pathway details employs a square $u \times u$ matrix of functions to modulate each element of the Hamiltonian, creating a dynamical system of dimension ud from the original d -dimensional one. The key point is that, while s modulation can completely distort the dynamics of the original system, the desired original pathway information is always preserved in a known manner.

Although in principle an infinite number of pathways contribute to any transition $|a\rangle \rightarrow |b\rangle$, in practice the bounded, finite-time nature of realistic controls implies that only a limited number of pathways will contribute significantly. The most detailed mechanism information resides in revealing the transition amplitudes of the full set of relevant pathways $\{U_{ba}^{n(l_1, \dots, l_{n-1})}\}$, but in most cases a lower-resolution picture may suffice or even be desirable. If there are many contributing pathways, then extraction of mechanism information in

full detail may be computationally expensive. Less detailed, lower-resolution information may give more insight into the control process. Thus, classes of pathways S_ν , $\nu = 1, 2, \dots$, may be defined where each class S_ν forms a subset of the original, full set of pathways, classified together because of some common characteristics. Each class has a transition amplitude

$$\tilde{U}_{ba}^\nu = \sum_{(a \rightarrow l_1, \dots, l_{n-1} \rightarrow b) \in S_\nu} U_{ba}^{n(l_1, \dots, l_{n-1})}, \quad (15)$$

where the summation is over all pathways ($a \rightarrow l_1, \dots, l_{n-1} \rightarrow b$) belonging to the class S_ν . Each pathway belongs to only one class. The goal in this case is to determine \tilde{U}_{ba}^ν directly without first extracting the individual terms in the summand on the right-hand side (RHS) of Eq. (15). Given the structure of Eqs. (9) and (15) it is possible to write the total amplitude as a sum over all pathway classes

$$U_{ba} = \sum_{\nu=1}^R \tilde{U}_{ba}^\nu, \quad (16)$$

where R is the number of significant pathway classes (which *a priori* is also unknown). An example considered later consists of classes defined by grouping pathways of the same order together. In that case we have

$$\tilde{U}_{ba}^\nu = \sum_{l_1, \dots, l_{\nu-1}=1}^d U_{ba}^{\nu(l_1, l_2, \dots, l_{\nu-1})}, \quad (17)$$

where all intermediate steps have been summed over. Modulation in the s domain yields

$$U_{ba}(s) = \sum_{\nu=1}^R \tilde{U}_{ba}^\nu M_{ba}^\nu(s), \quad (18)$$

where a suitable choice of $\{m_{ij}(s)\}$ ensures that all paths in S_ν have the same modulating function $M_{ba}^\nu(s)$, and that each function $M_{ba}^\nu(s)$, $\nu = 1, 2, \dots, R$, is unique—permitting the extraction of each amplitude \tilde{U}_{ba}^ν . Regardless of the specific form of pathway analysis, the structure of the resultant expression for $U_{ba}(s)$ remains the same [cf Eqs. (14) and (18)]. Considering the general case of Eq. (14) we require that the functions $M_{ba}^{n(l_1, \dots, l_{n-1})}$ be linearly independent over some specific domain of s . Ideally the functions are orthogonal under some suitably defined inner product such that

$$\langle M_{ba}^{n(l_1, \dots, l_{n-1})} | M_{ba}^{n'(l'_1, \dots, l'_{n-1})} \rangle = \delta_{n(l_1, \dots, l_{n-1}), n'(l'_1, \dots, l'_{n-1})}, \quad (19)$$

where the δ function is zero if any of the path indices differ or 1 if the indices are all the same. The notation $\langle | \rangle$ in Eq. (19) represents an inner product, e.g., an integration over s , possibly with a suitable weight function. Under the condition in Eq. (19),

$$U_{ba}^{n(l_1, \dots, l_{n-1})} = \langle M_{ba}^{n(l_1, \dots, l_{n-1})} | U_{ba} \rangle. \quad (20)$$

In the case that the functions $M_{ba}^{n(l_1, \dots, l_{n-1})}$ are just linearly independent, any of a variety of standard techniques from linear algebra may be applied to solve Eq. (14) for the amplitudes. In choosing an algorithm the goal is to obtain pathway information using a numerically stable technique for the deconvolution of Eq. (14) with a minimal number of samplings on the domain of s .

The choice of the set $\{m_{ij}(s)\}$ may be guided by a number of factors, including the fact that solving the Schrödinger equation can be expensive. This paper presents results obtained by using complex exponentials as a convenient set of modulating functions; however, no claim is made that this choice forms an optimum set of functions. Other possibilities (e.g., encoding with digital signals, wavelets, multiple modulation variables, etc.) are worthy of careful consideration.

IV. ALTERNATIVE CLASSES OF QUANTUM PATHWAY ANALYSES

This section will introduce distinct classes of quantum control mechanism analyses capable of revealing differing levels of detail. The examples in Sec. V illustrate each class of analysis.

A. The distribution of system orders

While the expansion in Eq. (9) always converges for realistic physical systems (see the Appendix), there is no way to know beforehand how many orders contribute significantly. This first class of mechanism analysis aims to identify the importance of the various orders contributing to U_{ba} . The information on the contributing orders is valuable as an initial glimpse at the mechanism and it also forms the starting point for the more detailed mechanism analyses to follow. This case corresponds to the situation in Eq. (17) and here we extract the desired information by modulating the entire interaction matrix by a single function $m(s)$:

$$V_I(t) \rightarrow V_I(t)m(s). \quad (21)$$

The integral corresponding to all n th-order pathways

$$\begin{aligned} \tilde{U}_{ba}^n &= \left(\frac{-i}{\hbar} \right)^n \langle b | \int_0^T \cdots \int_0^{t_2} V_I(t_n) \cdots V_I(t_1) dt_1 \cdots dt_n | a \rangle \\ &= \sum_{l_1, \dots, l_{n-1}=1}^d \int_0^T \cdots \int_0^{t_2} v_{bl_{n-1}}(t_n) \cdots v_{l_1 a}(t_1) dt_1 \cdots dt_n \end{aligned} \quad (22)$$

is modulated by a factor $m(s)^n$. Therefore $U_{ba}(s)$ can be written as

$$U_{ba}(s) = \sum_{n=1}^R \tilde{U}_{ba}^n m(s)^n, \quad (23)$$

which is a special case of Eq. (18). Although the number of significantly contributing pathways R is generally not known *a priori*, a reasonable estimate may be available (but is not required by the algorithm).

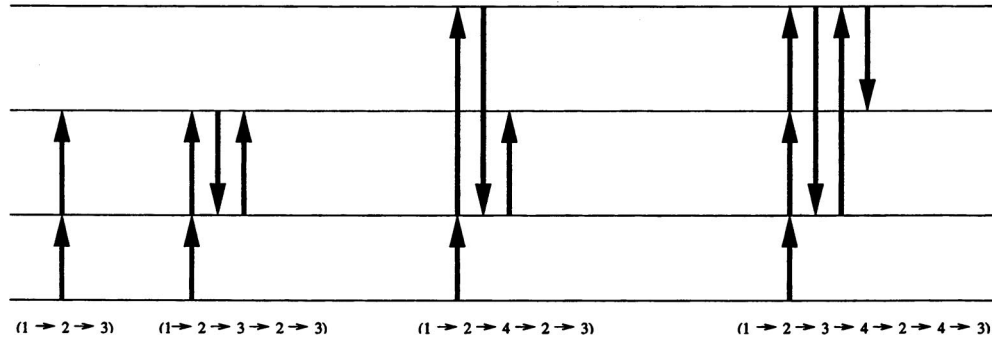


FIG. 3. Four examples of pathways with a net $1 \rightarrow 2 \rightarrow 3$ transition. All of them (and an infinite number of other pathways) belong to the same composite-pathway class $(1 \rightarrow 2 \rightarrow 3)^*$.

We choose $m(s) = e^{i\gamma s}$ ($\gamma = 2\pi/N$ for some suitable integer N) and evaluate $U_{ba}(s)$ at $s = 1, 2, \dots, N$. Then Eq. (18) becomes

$$U_{ba}(s) = \sum_{n=1}^R \tilde{U}_{ba}^n e^{2\pi i s n / N}, \quad s = 1, 2, \dots, N. \quad (24)$$

If $N \geq R$, then the coefficients may be computed by the inverse fast Fourier transform (FFT) of $U_{ba}(s)$, using the orthogonality relationship

$$\frac{1}{N} \sum_{s=1}^N [m^n(s)]^* m^l(s) = \delta_{nl}. \quad (25)$$

Since the value of R is not known beforehand, it is generally necessary to repeat the procedure with increasing N to ensure that all relevant order paths are accounted for. If $N < R$ then the high-order (frequency) terms can appear as low-order (frequency) terms due to aliasing. Convergence will be achieved when \tilde{U}_{ba}^n , for all relevant n , does not show significant change with increasing N . This procedure is computationally efficient as computations with increasing N may reuse all the previous N' points and only $N - N'$ new points need to be evaluated by solving Schrödinger's equation.

B. Revealing composite pathways

After classifying pathways according to their order by the procedure in Sec. IV A, further information can be extracted about the mechanism by decomposing the contributions within each order and recombining them in a different manner. A class of composite pathways is introduced for this purpose. The concept of a composite pathway is best illustrated by an example. Consider a four-level system where the control field drives the system from the initial state $|1\rangle$ to state $|3\rangle$. The overall amplitude of transition U_{31} may have multiple relevant pathways. In particular, consider four possible pathways $(1 \rightarrow 2 \rightarrow 3)$, $(1 \rightarrow 2 \rightarrow 3 \rightarrow 2 \rightarrow 3)$, $(1 \rightarrow 2 \rightarrow 4 \rightarrow 2 \rightarrow 3)$, and $(1 \rightarrow 2 \rightarrow 3 \rightarrow 4 \rightarrow 2 \rightarrow 4 \rightarrow 3)$. These pathways are shown in Fig. 3. All four paths (and an infinite number of other easily constructed paths) have the same net transition $1 \rightarrow 2 \rightarrow 3$ and differ only due to extra ‘‘rattling,’’ or Rabi flopping, where the pathway jumps from a state $|i\rangle$ to another state $|j\rangle$ and later jumps from $|j\rangle$ back to $|i\rangle$. In some

cases it is useful to know the total amplitude of pathways contributing to U_{31} which proceed via a given composite pathway regardless of how many times the pathway rattled around elsewhere. A later illustration will show that composite-pathway amplitudes can clearly reveal how optimal control theory tunes pathway amplitudes for the best use of constructive and destructive interference to reach the desired target.

Each composite-pathway class is denoted by the lowest-order pathway belonging to it, and marked with an asterisk. All paths with the net transition $(1 \rightarrow 2 \rightarrow 3)$ will be collectively denoted as contributing to the composite pathway $(1 \rightarrow 2 \rightarrow 3)^*$, and the transition amplitude of the composite pathway will be labeled similarly. Therefore the transition amplitude of the composite pathway $(1 \rightarrow 2 \rightarrow 3)^*$ is written as

$$\tilde{U}_{31}^{2(2)*} = U_{31}^{2(2)} + U_{31}^{4(2,3,2)} + U_{31}^{4(2,4,2)} + U_{31}^{4(2,3,4,2,4)} + \dots \quad (26)$$

Another separate class of composite pathways for the same overall transition $|1\rangle \rightarrow |3\rangle$ is $(1 \rightarrow 4 \rightarrow 2 \rightarrow 3)^*$, which contains the pathways $(1 \rightarrow 4 \rightarrow 2 \rightarrow 3)$, $(1 \rightarrow 4 \rightarrow 2 \rightarrow 4 \rightarrow 2 \rightarrow 3)$, etc.

In order to identify composite pathways we choose the following encoding scheme:

$$v_{ij} \rightarrow v_{ij} e^{i\gamma_{ij}s}, \quad (27a)$$

$$\gamma_{ij} = -\gamma_{ji}. \quad (27b)$$

This form of modulation preserves the Hermitian nature of the Hamiltonian. This scheme assigns the same overall modulation function of s to all paths belonging to the same composite pathway. For example, the amplitudes of the pathways $(1 \rightarrow 2 \rightarrow 3)$ and $(1 \rightarrow 2 \rightarrow 3 \rightarrow 2 \rightarrow 3)$ will have modulating functions $\exp\{i(\gamma_{12} + \gamma_{23})s\}$ and $\exp\{i(\gamma_{12} + \gamma_{23} + \gamma_{32} + \gamma_{23})s\} = \exp\{i(\gamma_{12} + \gamma_{23})s\}$, by virtue of the definition in Eq. (27b). The cancellation will occur for any rattling as a transition pair $i \rightarrow j$ and $j \rightarrow i$ will not shift the pathway frequency because of the condition imposed in Eq. (27b). Then we have

$$U_{ba}(s) = \sum_k \tilde{U}_{ba}^{(k)*} e^{i\gamma_k s}. \quad (28)$$

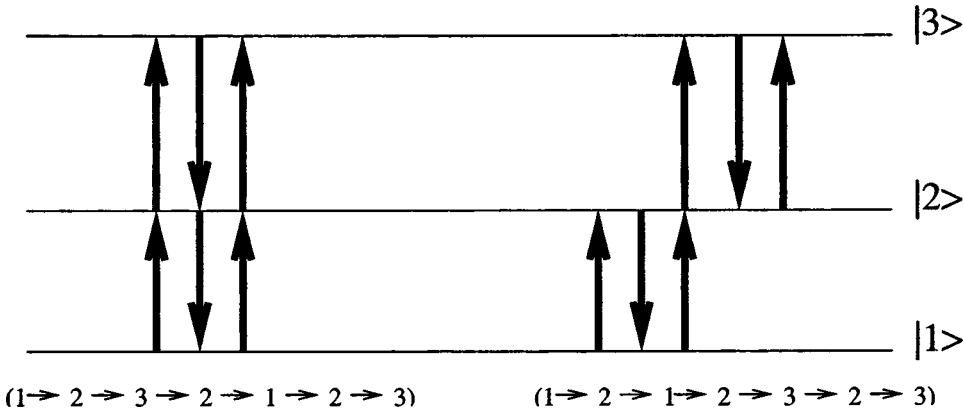


FIG. 4. Temporally distinguishable pathways like the pair shown here involve the same transitions, but in a different temporal sequence. A scalar modulation algorithm cannot separate them as they will always have the same associated scalar modulation function. The noncommutative modulation techniques of Sec. IV D can separate such transition amplitudes.

Each composite path labeled by k will have an associated frequency γ_k .

The inverse FFT can then be used to extract the individual composite amplitudes as follows. Choose $\{\gamma_{ij}\}$ (and hence $\{\gamma_k\}$) as integer multiples of some frequency γ_0 (as yet unknown) such that all significant composite pathways have a unique frequency assigned to them. First, the results of the algorithm of Sec. IV A are used to determine the list of possible significant pathways. For example, for a four-level system, in the analysis of $U_{41}(T)$, if the analysis of Sec. IV A shows that pathways up to third order contribute significantly then the possible composite pathways are $\{(1 \rightarrow 4)^*, (1 \rightarrow 2 \rightarrow 4)^*, (1 \rightarrow 3 \rightarrow 4)^*, (1 \rightarrow 2 \rightarrow 3 \rightarrow 4)^*, (1 \rightarrow 3 \rightarrow 2 \rightarrow 4)^*\}$. The set $\{\gamma_{ij}\}$ must then be assigned such that these composite pathways are at different frequencies $\{\gamma_k\}$. Then a convenient N (e.g., for the FFT we could choose a power of 2) is chosen such that $\gamma_k \leq N\gamma_0$ for all relevant k . Taking $\gamma_0 = 2\pi/N$ and evaluating Eq. (28) at $s = 1, 2, \dots, N$, we create a sequence whose FFT coefficients $\{\gamma_k\}$ are the transition amplitudes of the composite pathways.

C. Revealing rattling contributions to composite pathways

In some situations it may be desirable to further decompose the composite pathways of Sec. IV B to reveal the contributions from cases involving both $i \rightarrow j$ and $j \rightarrow i$ transitions. The rattling could be sequential, e.g., $(\dots i \rightarrow j \rightarrow i \dots)$ or separated $(i \rightarrow j \rightarrow k \rightarrow j \rightarrow i \dots)$. In order to reveal rattling the symmetry condition of Eq. (27b) is relaxed to keep just

$$v_{ij} \rightarrow v_{ij} e^{i\gamma_{ij}s}. \quad (29)$$

This encoding produces a non-Hermitian coupling matrix in Eq. (11). Pathways differing by rattles may now be at different frequencies (provided that the $\{\gamma_{ij}\}$ are appropriately chosen). For example, $(1 \rightarrow 2 \rightarrow 3)$ and $(1 \rightarrow 2 \rightarrow 3 \rightarrow 2 \rightarrow 3)$ will have modulating functions $\exp\{i(\gamma_{12} + \gamma_{23})s\}$ and $\exp\{i(\gamma_{12} + \gamma_{23} + \gamma_{32} + \gamma_{23})s\}$, respectively, which can now be distinct. An inverse FFT can again be used to extract pathway amplitudes after assigning $\{\gamma_{ij}\}$ such that all pathways up to the relevant order are at distinct frequencies (one exception to this procedure will be illustrated in Sec. IV D), by following operations identical to the one of Sec. IV B. In

practice, finding the transition amplitudes of all relevant pathways in this manner can be computationally formidable. Considering a four-level system evolving from $|1\rangle$ to $|4\rangle$ with pathways up to third order being relevant, there are ten possibly relevant pathways. The number of possible pathways increases rapidly with order much faster than the number of composite pathways (e.g., for order 8 there are 658 pathways but only 73 composite pathways). For high-dimensional systems with high-order pathway contributions, several options are available. It may often be advisable to stop at the composite-pathway level of analysis, which should give sufficient mechanism information. If more information is desired then the modulation can be applied selectively to only those matrix elements which correspond to the pathway(s) of interest. An extreme form of this logic may be applied by turning off all other transitions with the modulation $m_{ij} = 0$. For example, the transition amplitude of $(1 \rightarrow 4)$ can be identified by setting $m_{ij}(s) = 0$ for all coupling terms except v_{41} . This process turns off all pathways except the one of interest. Although $U_{41}(s)$ is highly distorted from the original amplitude U_{41} the information regarding the desired pathway will be retained. Results from the algorithm of Sec. IV B can be used to decide which pathways demand a full rattling analysis to reduce computational effort.

The more detailed algorithm of this section is unable to distinguish between pathways having the same transitions but ordered differently in time. An example is illustrated in Fig. 4. Since each pathway is labeled only in terms of its transitions, it is not possible to distinguish between such pathways by the methods introduced so far. The sum of the transition amplitudes of these paths will always be associated with the same overall modulating function. Such pathways will be referred to as temporally distinguishable pathways. Therefore the algorithm in this section classifies all temporally distinguishable pathways together. The decomposition of the time evolution operator can be written as

$$U_{ba}(s) = \sum_k \tilde{U}_{ba}^{n(k)T}, \quad (30)$$

where the additional notation $(k)^T$ has been introduced to denote a set of temporally distinguishable pathways.

D. Discriminating between temporally distinguishable pathways

Figure 4 shows two pathways that involve exactly the same transitions, but in a different temporal sequence. The two transition amplitudes $U_{31}^{6(2,3,2,1,2,3)}$ and $U_{31}^{6(2,1,2,3,2,3)}$ will, in general, have different contributions. However the algorithm in Sec. IV C cannot discriminate between them, and can only compute the sum of their amplitudes. The previous algorithm encoded each transition $i \rightarrow j$ through its modulating function $m_{ij}(s)$, and each pathway had a product of such modulating functions attached to it, reflecting the transitions it contained. However, temporally distinguishable transition pathways could not be discriminated from each other because the modulating functions commuted with each other, i.e., there was invariance to the time order of any two transitions such as $l \rightarrow k$ and $i \rightarrow j$ because $m_{lk}(s)m_{ij}(s)$

$=m_{ij}(s)m_{lk}(s)$. A noncommutative modulation scheme could discriminate amongst such temporally distinguishable pathways. Consider the noncommutative modulation scheme

$$v_{ij} \rightarrow v_{ij} m_{ij}(s) \mathbf{A}_{ij} \quad (31)$$

where \mathbf{A}_{ij} is a real, nonsymmetric, $u \times u$ matrix and the set $\{\mathbf{A}_{ij}\}$ is used in the overall encoding of the dynamics. If there are p temporally distinguishable pathways to separate, then u is the smallest integer such that $u^2 \geq p$. The matrices $\{\mathbf{A}_{ij}\}$ are independent of both t and s . This modulation scheme creates a new quantum system with dimension ud (where d was the dimension of the original system). The conditions on $\{\mathbf{A}_{ij}\}$ for successful separation of temporally distinguishable pathways will be made clear in the following analysis.

In the interaction picture the equation of motion for the new $ud \times ud$ evolution matrix U' has the form

$$\frac{dU'(t,s)}{dt} = \begin{pmatrix} v_{11}(t)\mathbf{A}_{11}m_{11}(s) & v_{12}(t)\mathbf{A}_{12}m_{12}(s) & \cdots & v_{1d}(t)\mathbf{A}_{1d}m_{1d}(s) \\ v_{21}(t)\mathbf{A}_{21}m_{21}(s) & v_{22}(t)\mathbf{A}_{22}m_{22}(s) & \cdots & v_{2d}(t)\mathbf{A}_{2d}m_{2d}(s) \\ \cdot & \cdot & \cdot & \cdot \\ \cdot & \cdot & \cdot & \cdot \\ v_{N1}(t)\mathbf{A}_{d1}m_{d1}(s) & v_{N2}(t)\mathbf{A}_{d2}m_{d2}(s) & \cdots & v_{NN}(t)\mathbf{A}_{dd}m_{dd}(s) \end{pmatrix} U'(t,s). \quad (32)$$

Instead of the scalar output $U_{ba}(s)$ from the evolution matrix we now have the analogous $u \times u$ submatrix:

$$\mathbf{U}'_{ba}(s) = \begin{pmatrix} U'_{(b-1)u+1,(a-1)u+1}(s) & \cdots & U'_{(b-1)u+1,au}(s) \\ \cdot & \cdots & \cdot \\ \cdot & \cdots & \cdot \\ U'_{bu,(a-1)u+1}(s) & \cdots & U'_{bu,au}(s) \end{pmatrix} \quad (33)$$

and $\mathbf{U}'_{ba}(s)$ can be written as

$$\mathbf{U}'_{ba}(s) = \sum_{n=1}^{\infty} \sum_{l_1, l_2, \dots, l_{n-1}=1}^d U_{ba}^{n(l_1, l_2, \dots, l_{n-1})} \mathbf{D}_{ba}^{n(l_1, \dots, l_{n-1})} \times M_{ba}^{n(l_1, l_2, \dots, l_{n-1})}(s), \quad (34)$$

where

$$\mathbf{D}_{ba}^{n(l_1, \dots, l_{n-1})} = \mathbf{A}_{bl_{n-1}} \mathbf{A}_{l_{n-1}l_{n-2}} \cdots \mathbf{A}_{l_1 a} \quad (35)$$

are $u \times u$ matrices and the M functions are defined exactly as before. Using the same $m_{ij}(s)$ as in Sec. IV C makes each M function a complex exponential such that

$$\mathbf{U}'_{ba}(s) = \sum_{n=1}^{\infty} \sum_{l_1, l_2, \dots, l_{n-1}=1}^d U_{ba}^{n(l_1, l_2, \dots, l_{n-1})} \times \mathbf{D}_{ba}^{n(l_1, \dots, l_{n-1})} e^{is\gamma_n(l_1, l_2, \dots, l_{n-1})}. \quad (36)$$

Now each pathway has a label consisting of two parts—a scalar s modulation function and a matrix \mathbf{D} . Since all the temporally distinguishable pathways have the same scalar modulating function, they sit on the same frequency, e.g., γ_x . However, the different ordering of transitions is now reflected in the fact that $\mathbf{A}_{lm}\mathbf{A}_{ij} \neq \mathbf{A}_{ij}\mathbf{A}_{lm}$. Hence each temporally distinguishable pathway will have a different matrix \mathbf{D} associated with it.

An inverse FFT of each element of the $u \times u$ matrix $\mathbf{U}'_{ba}(s)$ can be used to pick the required frequency component γ_x , generating a matrix \mathbf{K} . If the transition amplitudes of the p temporally distinguishable transition pathways are $U_{ba}^{m(l_1^1, \dots, l_{n-1}^1)}$, $U_{ba}^{m(l_2^1, \dots, l_{n-1}^1)}$, ..., $U_{ba}^{m(l_2^p, \dots, l_{n-1}^p)}$, then after the FFT we get the $u \times u$ matrix equation

$$\mathbf{K} = \sum_{i=1}^p U_{ba}^{m(l_1^i, \dots, l_{n-1}^i)} \mathbf{D}_{ba}^{m(l_1^i, \dots, l_{n-1}^i)}. \quad (37)$$

With appropriate choice of the matrices $\{\mathbf{A}_{ij}\}$, the matrices $\{\mathbf{D}_{ba}^{m(l_1^i, \dots, l_{n-1}^i)}\}$ will be linearly independent and Eq. (37) will give a system of u^2 ($> p$) linear equations in p un-

knows $\{U_{ba}^{m(l_1, \dots, l_{n-1})}\}$, $i=1, 2, \dots, p$, that can be solved for the amplitudes of individual temporally distinguishable pathways.

V. ILLUSTRATIONS OF CONTROL PATHWAY ANALYSIS

The mechanism analysis procedures of Sec. IV were applied to several model quantum systems. In all cases the eigenstates of the unperturbed Hamiltonian were used to represent the evolution. However, other bases could be used if transitions between them can be given suitable physical meaning. All the analyses were initiated by determining significant pathway orders as explained in Sec. IV A. For systems with fewer than four states the non-Hermitian modulation scheme of Sec. IV C was applied directly after this step because the number of pathways was quite small. For larger systems the transition amplitudes for the composite pathways were computed by the algorithm of Sec. IV B, and then the dominant composite pathways were analyzed by the procedure of Sec. IV C to reveal the underlying dynamical rattling.

The numerical integration of the Schrödinger equation was done by approximating the interaction Hamiltonian as piecewise constant:

$$U(T) = \tau \exp\left(-\frac{i}{\hbar} \int_0^T V_I(t) dt\right) \approx \prod_{n=1}^{T/\Delta t} \exp\left(-\frac{i}{\hbar} V_I(t_n) \Delta t\right), \quad (38)$$

$$t_n = n \Delta t,$$

where τ is the time-ordering operator. The matrix exponential may be computed by Hamiltonian diagonalization. However, in some of the proposed modulation schemes the encoded Hamiltonian is non-Hermitian, and it is possible that the matrix may not always be diagonalizable. Therefore, Padé approximants [24] were used to compute all matrix exponentials.

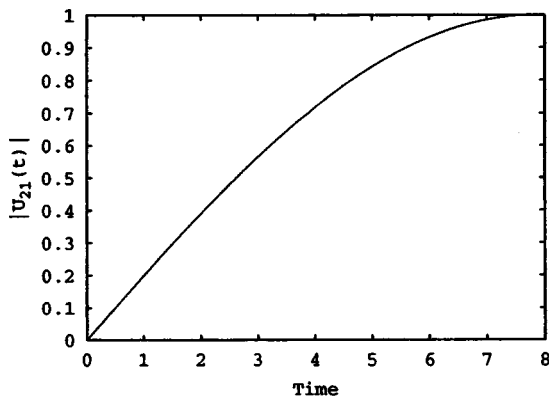


FIG. 5. The magnitude of the transition amplitude $|U_{21}(t)|$ for the two-level test case as a function of time in dimensionless units. The monotonic rise in amplitude hides the true multiphoton contributions shown in Table I.

TABLE I. The transition amplitudes for the two-level system in Fig. 5.

Path	Amplitude
(1→2)	-1.57i
(1→2→1→2)	0.65i
(1→2→1→2→1→2)	-0.08i

A. Resonant nonoptimally controlled models

The first class of systems analyzed by Hamiltonian encoding used nonoptimal fields, resonantly coupled within the rotating-wave approximation (RWA). Such simple model cases produce time-independent coupling matrices in Eq. (10), allowing for an alternative, direct determination of the pathway transition amplitudes for algorithm verification. The results are also physically instructive. For a time-independent matrix V_I the transition amplitude for a path of order n from Eq. (8) becomes

$$\begin{aligned} U_{ab}^{n(l_1, \dots, l_{n-1})} &= \int_0^T \int_0^{t_n} \cdots \int_0^{t_2} v_{b l_{n-1}}(t_n) v_{l_{n-1} l_{n-2}}(t_{n-1}) \cdots \\ &\quad \times v_{l_1 a}(t_1) dt_1, \dots, dt_{n-1} dt_n \\ &= v_{b l_{n-1}} v_{l_{n-1} l_{n-2}} \cdots v_{l_1 a} \frac{T^n}{n!}. \end{aligned} \quad (39)$$

The first application is to a two-level system described in dimensionless units, with the field amplitude adjusted for complete transfer of population from level $|1\rangle$ to $|2\rangle$. A plot of $|U_{21}(t)|$ is shown in Fig. 5. The monotonically increasing

TABLE II. The pathway amplitudes for the three-level system.

Pathway	Amplitude ^a	Amplitude ^b
(1→2→3)	-2.250	-2.250
(1→2→1→2→3)	1.688	1.688
(1→2→3→2→3)	0.422	0.422
(1→2→1→2→1→2→3)	-0.506	-0.506
(1→2→1→2→3→2→3) ^c	-0.253	-0.127
(1→2→3→2→1→2→3) ^c	-0.253	-0.127
(1→2→1→2→1→2→1→2→3)	0.081	0.081
Total	-0.819 ^d	-0.819

^aCalculated by the encoding algorithm of Sec. IV C.

^bThe true values from Eq. (39).

^cThese two pathways are temporally distinguishable and cannot be separated by scalar encoding algorithms. The computed amplitude, which is the coefficient of the associated modulating function $M_{31}^{6(2,1,2,3,2)}(s) = M_{31}^{6(2,3,2,1,2)}(s)$, will be the sum of the two separate amplitudes. The sum shown in the table takes this into account and adds in the contribution (c) only once.

^dThe sum of the amplitudes should give the total value of $U_{31}(t) = -0.7912$. The observed mismatch arises because the table only includes pathways with amplitudes satisfying $|U_{31}^{(k)}| \geq 0.08$.

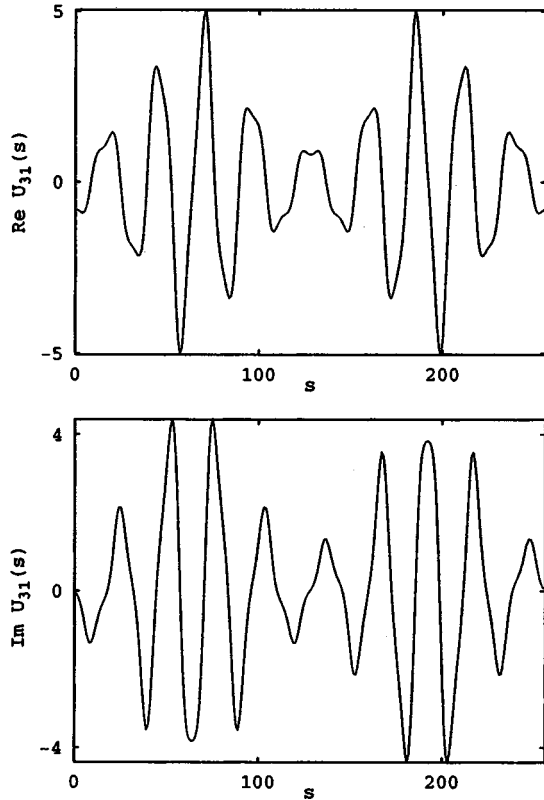


FIG. 6. A plot of the real and imaginary parts of $U_{31}(s)$ for the three-level case with the coupling matrix in Eq. (41). Information about the pathways for $|1\rangle \rightarrow |3\rangle$ is revealed by a FFT decoding of this output signal as shown in Fig. 7. The variable s is dimensionless.

transfer of population from $|1\rangle$ to $|2\rangle$ might suggest that only a one-photon process is involved, but the pathway analysis results in Table I show a significant contribution from the rattling pathway ($1 \rightarrow 2 \rightarrow 1 \rightarrow 2$). The numerical pathway identification results agree exactly with the simple analytical expression in Eq. (39) that the different pathway transition amplitudes arise from the Taylor series expansion of $-i \sin(\pi/2)$:

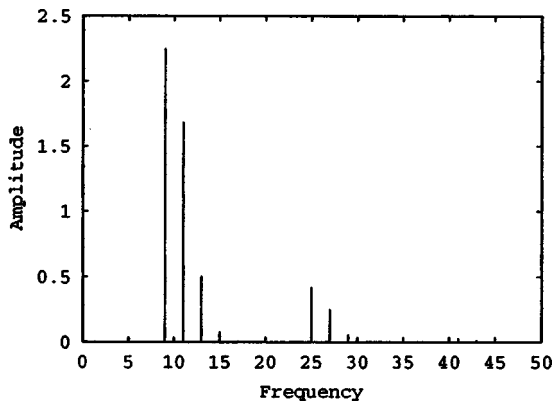


FIG. 7. The magnitude of the FFT of the signal in Fig. 6. The spectrum corresponds to the amplitudes listed in Table II. The frequency is dimensionless.

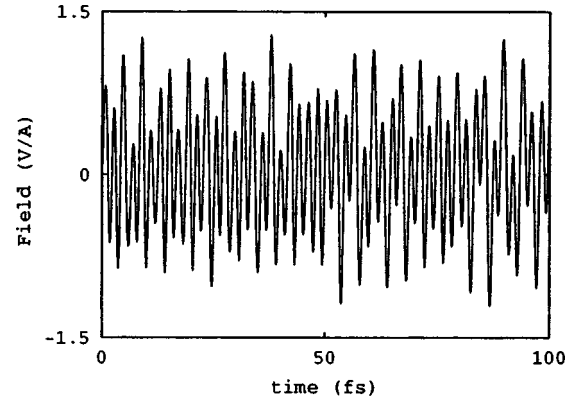


FIG. 8. The control field designed using optimal control for transfer from $|1\rangle$ to $|3\rangle$ for the four-level system.

$$U_{21}(T) = \left(\frac{-i}{\hbar} V_{21} \right) T + \left(\frac{-i}{\hbar} \right)^3 \frac{V_{21} V_{12} V_{21} T^3}{3!} + \dots \quad (40)$$

with $(1/\hbar)V_{12}T = \pi/2$.

The pathway analysis was then applied to another simple system with the v matrix of Eq. (10) in the RWA having the form

$$v = i \begin{pmatrix} 0 & 0.2 & 0 \\ 0.2 & 0 & 0.1 \\ 0 & 0.1 & 0 \end{pmatrix}, \quad (41)$$

where the units used are arbitrary. The system is initially in the state $|1\rangle$, and the dynamics was followed out to time $T = 15$, where $|U_{31}| = 0.79$. The analysis of Sec. IV A for the $|1\rangle \rightarrow |3\rangle$ transition showed that pathways up to order 8 contributed significantly for U_{31} . The significant pathways and their transition amplitudes are shown in Table II. Paths including $1 \rightarrow 3$ or $3 \rightarrow 1$ transitions do not arise in this case as $v_{13}(t) = v_{31}(t) = 0$ for all t . $U_{31}(s)$ is plotted in Fig. 6. The magnitude of the inverse FFT of $U_{31}(s)$ is shown in Fig. 7, which corresponds to the results in Table II. The amplitudes determined by using the analysis of Sec. IV C fully agree with those obtained by a direct evaluation of Eq. (39). Table II also shows two temporally distinguishable pathways

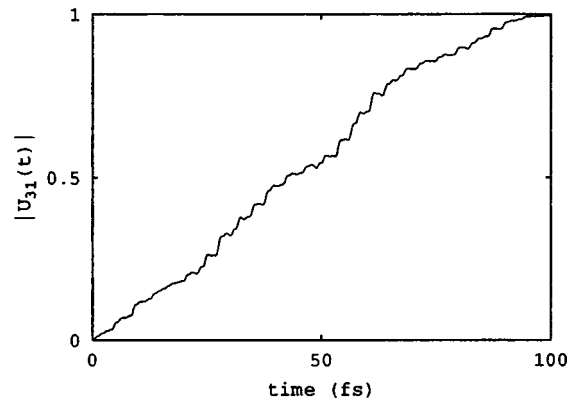


FIG. 9. Population in level $|3\rangle$ as a function of time with the four-level system driven by the optimal field in Fig. 8.

TABLE III. Moduli of the significantly contributing pathway orders for the transition $|1\rangle \rightarrow |3\rangle$ with the four-level system driven by the optimal field.

Order	Modulus
1	0.85
2	1.36
3	0.85
4	0.73
5	0.25
6	0.15
7	0.037
8	0.017

whose amplitudes were successfully separated (details not shown here) using the noncommutative encoding scheme of Sec. IV D. The scalar encoding scheme gives the sum of their amplitudes as part of the temporally distinguishable pathway class.

B. Mechanisms of systems driven by optimal control fields

The pathway analysis algorithms are now applied to two examples where the field has been computed using optimal control theory [1,4–6], without the RWA. The first case is a four-level system [25] with the goal being population transfer from level $|1\rangle$ to $|3\rangle$, along with a small cost to the field fluence. The field computed using a local (steepest-descent) optimization algorithm [1] is shown in Fig. 8. The population in state $|3\rangle$, shown as a function of time in Fig. 9, was 0.99 at the target time. The algorithm of Sec. IV A was first applied to identify the orders of the significant pathways and the results are shown in Table III. Following the results in the table, the more detailed mechanism analysis neglected pathways of order 7 and greater.

The transition amplitudes of the composite pathways, computed using the algorithm of Sec. IV B, is shown in

TABLE IV. Moduli and phases of the composite pathways for the transition $|1\rangle \rightarrow |3\rangle$ with the four-level system driven by the optimal field.

Path	Modulus	Phase (rad) ^a
$(1 \rightarrow 3)^*$	0.24	-2.51
$(1 \rightarrow 2 \rightarrow 3)^*$	0.61	-2.59
$(1 \rightarrow 4 \rightarrow 3)^*$	0.15	-2.64
$(1 \rightarrow 2 \rightarrow 4 \rightarrow 3)^*$	0.000 47	-2.92

^aThe optimal field tends to align the phases for efficient constructive interference.

Table IV. The most important composite pathway is $(1 \rightarrow 2 \rightarrow 3)^*$. The table indicates that the phases of the major pathway amplitudes are very well aligned; hence the composite pathways interfere constructively to reach the target. This behavior is a consequence of employing optimal control to attain the best possible outcome; the fluence cost in the optimal control algorithm likely aids this process by attempting to make the transfer efficient. It is convenient to define an amplitude alignment parameter η :

$$\eta = \frac{\left| \sum_n U_{ba}^{(n)*} \right|}{\sum_n |U_{ba}^{(n)*}|}, \tag{42}$$

which provides a measure of the constructive interference among the composite pathways. For the three major composite pathways η was 0.999, which means that they show almost perfect constructive interference. A similar analysis was also done for the transition $|1\rangle \rightarrow |4\rangle$. The optimal field was designed to maximize $|U_{31}(T)|$, and the population in the state $|4\rangle$ was $|U_{41}(T)|^2 = 0.01$. The composite pathways for this transfer destructively interfere in order to ensure near-zero final population in $|4\rangle$, resulting in the major composite

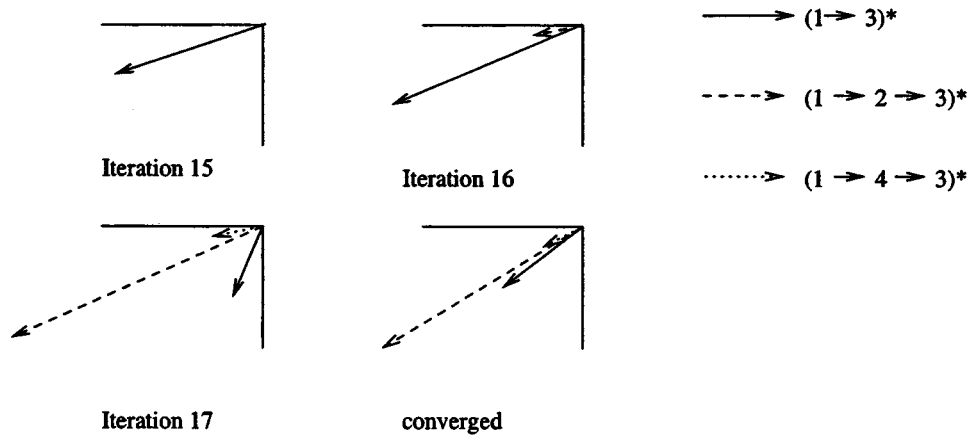


FIG. 10. The introduction of different composite-pathway amplitudes shown in the complex plane for the four-level system where the goal is optimal transfer of population for $|1\rangle \rightarrow |3\rangle$. The initial field guess had no pathways connecting $|1\rangle$ to $|3\rangle$. For iterations 1 through 15 only one composite pathway $(1 \rightarrow 3)^*$ was significant. The optimization algorithm first introduces the relevant composite pathways, and then optimally aligns them at convergence. The final converged composite amplitudes are almost completely aligned, and are shown slightly separated here for graphical clarity. The key for the composite-pathway fonts is shown on the right.

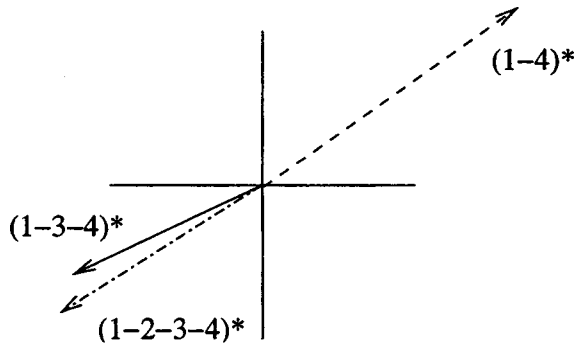


FIG. 11. Destructive interference of pathways in the nontarget state $|4\rangle$ for the four-level system. The pathways shown in the complex plane for the $|1\rangle \rightarrow |4\rangle$ transfer do not cancel out completely as several smaller-amplitude pathways also contribute significantly to ensure no net population in $|4\rangle$.

paths having $\eta=0.03$ for the $|1\rangle \rightarrow |4\rangle$ transition. The mechanism analyses for $U_{31}(T)$ and $U_{41}(T)$ in this example demonstrate how the optimal control process seeks out a control field $\mathcal{E}(t)$ to manipulate multiple pathways in a fashion to yield constructive interference in the desired final state and destructive interference in the other states. This point is illustrated graphically in Figs. 10 and 11.

All pathways up to order 5 including rattling for $|1\rangle \rightarrow |3\rangle$ were decomposed according to the procedure of Sec. IV C, and pathways up to order 4 are shown in Table V. This analysis captures most of the processes, but Table III shows that additional processes also occur out to order 6. Some sixth-order pathway transition amplitudes were also computed but the trend indicated that there is no sixth-order pathway of high amplitude; the overall contribution of the sixth-order terms is because of the large number of participating pathways rather than the presence of a few significant pathways.

It is evident from Table V that the decomposed pathways are not aligned, unlike what is observed for the composite

TABLE V. Moduli and phases for all significant pathways up to order 4 for the transition $|1\rangle \rightarrow |3\rangle$ in the four-level system. A relationship exists amongst the phases of pathways marked with the same symbol (\dagger, \ddagger) as explained in the text, resulting in these pathways not being aligned like the composite pathways.

Path	Modulus	Phase
$(1 \rightarrow 3)$	0.85	$-2.8 \dagger$
$(1 \rightarrow 2 \rightarrow 3)$	1.08	$-2.64 \ddagger$
$(1 \rightarrow 4 \rightarrow 3)$	0.28	-2.63
$(1 \rightarrow 2 \rightarrow 1 \rightarrow 3)$	0.31	$0.316 \dagger$
$(1 \rightarrow 3 \rightarrow 1 \rightarrow 3)$	0.10	$0.338 \dagger$
$(1 \rightarrow 3 \rightarrow 2 \rightarrow 3)$	0.26	$0.179 \dagger$
$(1 \rightarrow 4 \rightarrow 1 \rightarrow 3)$	0.16	$-0.773 \dagger$
$(1 \rightarrow 2 \rightarrow 1 \rightarrow 2 \rightarrow 3)$	0.21	$0.444 \ddagger$
$(1 \rightarrow 2 \rightarrow 3 \rightarrow 1 \rightarrow 3)$	0.10	$0.541 \ddagger$
$(1 \rightarrow 2 \rightarrow 3 \rightarrow 2 \rightarrow 3)$	0.18	$0.595 \ddagger$
$(1 \rightarrow 4 \rightarrow 1 \rightarrow 2 \rightarrow 3)$	0.12	$-0.695 \ddagger$

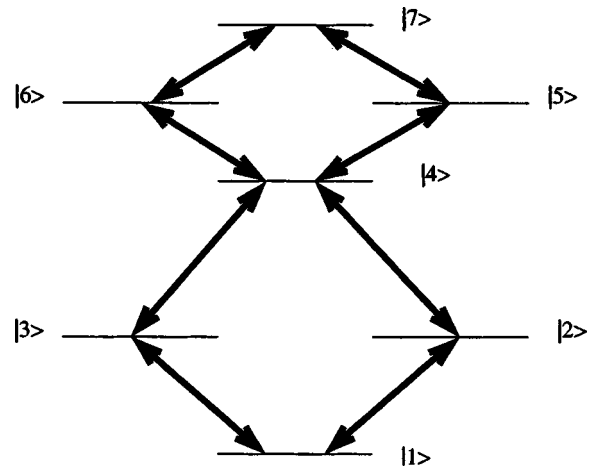


FIG. 12. The energies and allowed couplings for the seven-level system. The goal is population transfer from $|1\rangle$ to $|7\rangle$.

pathways, possibly implying that the optimization algorithm is missing an opportunity to work with constructive interferences. However, this view is misleading as there is a concealed relation between the phases of the pathways contributing to a single composite-pathway amplitude. This relationship can be qualitatively understood by considering a resonant RWA analysis of the analogous pathway amplitudes in Eq. (39). Consider the pathways $(1 \rightarrow 3)$ and $(1 \rightarrow 3 \rightarrow 2 \rightarrow 3)$, with their transition amplitudes

$$U_{31}^1 = \left(\frac{-i}{\hbar} \right) V_{31} T, \quad (43)$$

$$U_{31}^{3(3,2)} = \left(\frac{-i}{\hbar} \right)^3 V_{32} V_{23} V_{31} \frac{T^3}{6}, \quad (44)$$

where v_{ij} is explicitly written as $(-i/\hbar)V_{ij}$ in order to illustrate the connection between the phases. Since the phase of $(-i/\hbar)^2 V_{32} V_{23}$ is π , these two pathways will always be exactly out of phase. The actual optimally controlled dynamics of the example in Table V is more complex, but on examination the same pair of pathways (labeled with \dagger) shows this

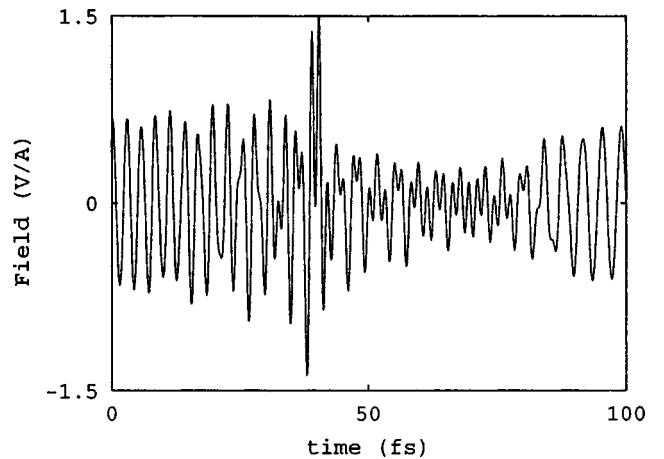


FIG. 13. The optimal field for making the transition $|1\rangle \rightarrow |7\rangle$ for the seven-level system of Fig. 12.

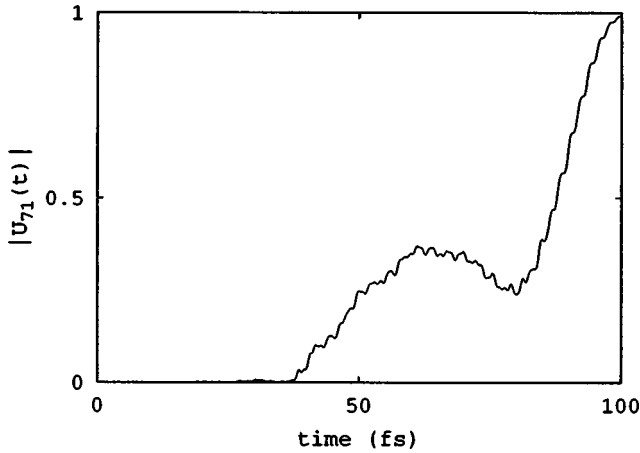


FIG. 14. Population in level $|7\rangle$ as a function of time with the seven-level system driven by the optimal field in Fig. 13.

behavior. It is also observed to different degrees among other pairs with a similar relation (see the paths labeled with ‡).

The pathway analysis can also be performed at intermediate iteration steps during the optimization process along the way to the optimum field to give further insight. In the present case after 15 iterations, the population in level $|3\rangle$ started to become significant (15%). At that point the composite-pathway analysis showed that only the $(1 \rightarrow 3)^*$ processes were significant. Iteration 16 produced a 34% transfer of the population and showed that, while $(1 \rightarrow 3)^*$ was dominant, the optimally controlled dynamics had started to use other pathways as well. On the next iteration a sudden jump in the population transfer from 34% to 80% was observed, accompanied by an increase in the contribution of higher-order composite pathways $(1 \rightarrow 2 \rightarrow 3)^*$, etc. The alignment was $\eta = 0.87$ for the composite pathways when all three major composite pathways are introduced (iteration 17), with η becoming 0.999 at convergence. Therefore, the optimization process consists of two cooperating features: (i) the introduction of different composite pathways, and (ii) their alignment for constructive interference at the target state. Figure 10 shows how the optimal control algorithm achieves constructive interference in the desired state $|3\rangle$ while Fig. 11 shows destructive interference in the nontarget state $|4\rangle$.

TABLE VI. The distribution of significant pathway orders in the seven-level system of Fig. 12 due to the optimal field of Fig. 13.

Order	Amplitude
4	5.2
5	0
6	7.5
7	0
8	4.7
9	0
10	1.7
11	0
12	0.4

TABLE VII. Amplitudes and phases of significant composite pathways for the seven-level system. The composite pathways are aligned.

Pathway	Amplitude	Phase
$(1 \rightarrow 2 \rightarrow 4 \rightarrow 5 \rightarrow 7)^*$	0.226	-0.417
$(1 \rightarrow 2 \rightarrow 4 \rightarrow 6 \rightarrow 7)^*$	0.256	-0.414
$(1 \rightarrow 3 \rightarrow 4 \rightarrow 5 \rightarrow 7)^*$	0.224	-0.413
$(1 \rightarrow 3 \rightarrow 4 \rightarrow 6 \rightarrow 7)^*$	0.255	-0.412
$(1 \rightarrow 2 \rightarrow 4 \rightarrow 3 \rightarrow 1 \rightarrow 2 \rightarrow 4 \rightarrow 5 \rightarrow 7)^*$	0.001	0.085

The pathway analysis algorithms were also applied to a seven-level system [26] shown in Fig. 12 governed by an optimal control field aiming to transfer population from $|1\rangle$ to $|7\rangle$. The system is slightly asymmetric because of the dipole coupling matrix elements. The optimal field shown in Fig. 13 produced 98% population in the target state $|7\rangle$, and the population as a function of time is shown in Fig. 14.

The main contributing pathway orders for the transition $|1\rangle \rightarrow |7\rangle$ are shown in Table VI using the algorithm of Sec. IV A. Due to the allowed couplings at least four steps are required to get from $|1\rangle$ to $|7\rangle$, as seen in the table. The four major composite pathways are shown in Table VII, and they are all in phase with $\eta = 0.9999$, again showing the tendency of optimal control to align the composite pathways. Table VI shows paths of orders 6, 8, and 10 as significant, implying that the control mechanism consists of the four simple direct pathways as well as up to three rattlings, with the pathways containing one rattle actually being more important than the direct pathways. The coupling diagram of Fig. 12, the distribution of orders in Table VI, and the composite pathways in Table VII provide a clear physical picture of the mechanism. The last row of Table VII shows a weak but physically interesting pathway traced out in Fig. 15 as containing a closed loop of couplings $(1 \rightarrow 2 \rightarrow 4 \rightarrow 3 \rightarrow 1)$ followed by transfer of amplitude to $|7\rangle$ by $(1 \rightarrow 2 \rightarrow 4 \rightarrow 5 \rightarrow 7)$.

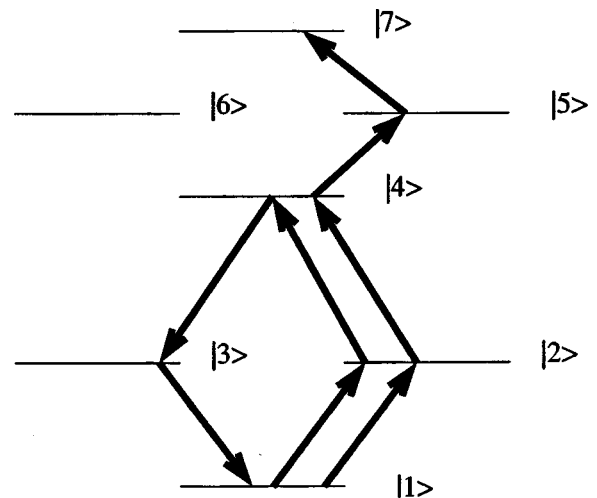


FIG. 15. A physically interesting (but low-amplitude) eighth-order composite pathway which involves looping around once $(1 \rightarrow 2 \rightarrow 4 \rightarrow 3 \rightarrow 1)$ before proceeding to the final state $(1 \rightarrow 2 \rightarrow 4 \rightarrow 5 \rightarrow 7)$.

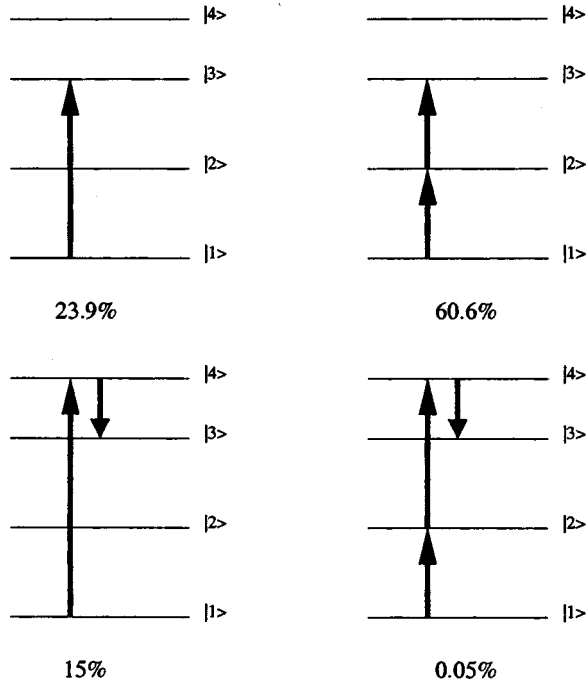


FIG. 16. The percentage contributions of the various composite-pathway moduli to the optimally induced transition $|1\rangle \rightarrow |3\rangle$ for the four-level system.

Since the optimal control fields tend to produce phase-aligned composite pathways in the target state, it follows that $U_{ba} = \sum_k |U_{ba}^{C(k)}| e^{i\phi_{ba}^{C(k)}} \approx e^{i\phi_{ba}} \sum_k |U_{ba}^{C(k)}|$, where the k th composite pathway has the phase $\phi_{ba}^{C(k)}$ and the phases are essentially a constant ϕ_{ba} . Therefore each composite pathway can be assigned a percentage contribution $100 |U_{ba}^{(k)*}| / \sum_{k'} |U_{ba}^{(k')*}|$ in achieving the final state. Figures 16 and 17 show the importance of the various composite pathways for the optimal control of the optimally controlled four- and seven-level systems, respectively. While the four-level system has a dominant composite pathway, the seven-level system, with its high degree of symmetry, uses all possible composite pathways almost equally.

VI. CONCLUSIONS

The pathway analysis algorithms introduced in the paper provide an efficient and thorough means to reveal quantum-mechanical control mechanisms. Defining mechanisms in terms of pathways is quite natural and allows for clear meaning to be given to the notions of constructive and destructive interference in controlling quantum systems. Most significantly, the mechanism analysis can be carried out in stages ranging from just revealing the order of interactions involved all the way out to the highest level of detail, identifying each individual contributing pathway amplitude. The pathway algorithms are especially efficient if only a few pathways are desired for analysis. In this case the modulating functions may be set to zero, $m_{ij} = 0$, for all transitions *not* involved in the desired pathways. This rather extreme case would lead to an encoded Hamiltonian that would have drastically different

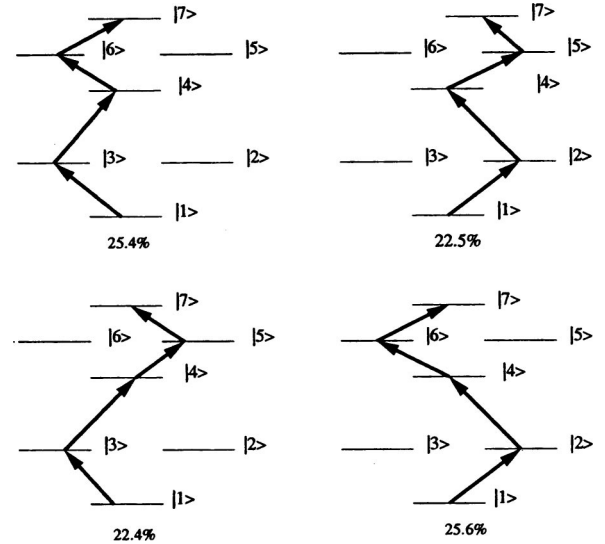


FIG. 17. The percentage contributions of the various composite-pathway moduli to the optimally induced transition $|1\rangle \rightarrow |7\rangle$ for the seven-level system.

dynamics, while still preserving the desired pathway information. A balance exists between the level of detail and the computational effort involved.

The algorithms introduced here might be improved in a number of ways. Ultimately, optimal criteria could be applied to determine the best encoding functions that balance numerical efficiency and stability. Notwithstanding these refinements, the Fourier-based procedures utilized in this paper are practical and ready for use in various applications. In extending the analyses to other systems it would be valuable to verify the generality of the observations regarding the alignment of composite pathways observed here.

Normally a mechanistic analysis would be performed at the last stage after obtaining an optimal control field. However, other applications can also be envisioned. For example, if some state (or pathway) is to be avoided during the controlled dynamics, then the mechanism analysis could be performed in tandem with the optimal control design. In this case pathway information would actually enter into the control-design cost function. Regardless of the applications, the conceptual tools introduced here should provide the means to reveal the underlying physics operating in the controlled manipulation of quantum systems.

ACKNOWLEDGMENTS

This work was supported by the National Science Foundation and the U.S. Department of Defense.

APPENDIX

The appendix addresses the convergence behavior of the Dyson series under normal physical conditions (including modulation). Consider the equation

$$\frac{dU}{dt} = V(t,s)U, \quad U(0) = 1, \quad (\text{A1})$$

where U and V are $d \times d$ matrices, and $V(t,s)$ incorporates modulation. The Dyson expansion for the solution of Eq. (A1) is

$$U(t,s) = I + \int_0^t V(t_1,s) dt_1 + \int_0^t V(t_2,s) \int_0^{t_2} V(t_1,s) dt_1 dt_2 + \dots \quad (\text{A2})$$

The physical systems in this paper are all of finite dimension d . The control field is always bounded in magnitude and on for a finite time T , and the modulation functions are also bounded from above. The dimension d either is fixed on physical grounds by H_0 or is an effective dimension beyond which no significant dynamics exists for the particular control problem. For such systems, $\|V(t,s)\|$ is bounded from above and nonzero over only a finite interval $[0,T]$. The expansion of Eq. (A2) always converges under these conditions. Hence, Eqs. (9) and (14) are mathematically meaningful and converge for any set of modulating functions $\{m_{ij}\}$ for all s where the m_{ij} are finite. A crude upper bound on Eq. (14) can be estimated as follows. Consider $w > 0$ to satisfy $w > |v_{ij}(t)m_{ij}(s)| \forall i,j,t,s$, which is possible as the elements of V are all bounded and nonzero for only a finite time interval $[0,T]$. Then each term in Eq. (12) may be bounded as

$$\left| \int_0^T \dots \int_0^{t_n} v_{bl_{n-1}}(t_n) m_{bl_{n-1}}(s) \dots v_{l_1 a}(t_1) m_{l_1 a}(s) dt_1 \dots dt_n \right| \leq \int_0^T \int_0^{t_n} \dots \int_0^{t_2} w w \dots w dt_1 \dots dt_{n-1} dt_n = \frac{w^n T^n}{n!}. \quad (\text{A3})$$

For n th order in the Dyson series there are $n-1$ intermediate steps each of which can be independently varied from 1 to d ; therefore there are d^{n-1} such integrals. Hence

$$|U_{ba}(s)| \leq \sum_{n=1}^{\infty} \sum_{l_1, \dots, l_{n-1}=1}^d |U_{ba}^{n(l_1, \dots, l_{n-1})} M_{ba}^{n(l_1, \dots, l_{n-1})}(s)| \leq \sum_{n=1}^{\infty} \frac{w^n d^{n-1} T^n}{n!} = \frac{1}{d} \sum_{n=1}^{\infty} \frac{w^n d^n T^n}{n!} = \frac{1}{d} (e^{wdT} - 1). \quad (\text{A4})$$

Since the series on the RHS of Eq. (14) is absolutely bounded from above, it converges.

The actual necessary condition on $V(t,s)$ for convergence is less stringent than the one imposed here [27], but this bound suffices to make the point about convergence behavior. Finally, the convergence of Eq. (A2) is consistent with the simple physical statement that in any real experiment only a finite number of photons will enter or leave the system due to the applied control field.

-
- [1] S. Shi and H. Rabitz, *J. Chem. Phys.* **92**, 364 (1989).
 [2] R. S. Judson and H. Rabitz, *Phys. Rev. Lett.* **68**, 1500 (1992).
 [3] W. S. Warren, H. Rabitz, and M. Dahleh, *Science* **259**, 1581 (1993).
 [4] R. Kosloff, S. Rice, P. Gaspard, S. Tersigni, and D. Tannor, *Chem. Phys.* **139**, 201 (1989).
 [5] S. Shi, A. Woody, and H. Rabitz, *J. Chem. Phys.* **88**, 6870 (1988).
 [6] H. Rabitz and W. Zhu, *Acc. Chem. Res.* **33**, 572 (2000).
 [7] H. Rabitz, R. de Vivie-Riedle, M. Motzkus, and K. Kompa, *Science* **288**, 824 (2000).
 [8] A. Assion *et al.*, *Science* **282**, 919 (1998).
 [9] D. Zeidler, S. Frey, K. L. Kompa, and M. Motzkus, *Phys. Rev. A* **64**, 23 420 (2001).
 [10] R. Bartels *et al.*, *Nature (London)* **406**, 164 (2000).
 [11] J. Kunde *et al.*, *J. Opt. Soc. Am. B* **18**, 872 (2001).
 [12] R. J. Levis, G. M. Menkir, and H. Rabitz, *Science* **292**, 709 (2001).
 [13] D. Zeidler *et al.*, *J. Chem. Phys.* **116**, 5231 (2002).
 [14] J. Herek *et al.*, *Nature (London)* **417**, 533 (2002).
 [15] S. Vajda, *Habilitation thesis*, Freie Universität Berlin, 2002.
 [16] J. M. Geremia, W. Zhu, and H. Rabitz, *J. Chem. Phys.* **13**, 10 841 (2000).
 [17] A. Mitra and H. Rabitz (unpublished).
 [18] J. J. Sakurai, *Modern Quantum Mechanics* (Addison-Wesley, Reading, MA, 1994).
 [19] R. P. Feynmann and A. R. Hibbs, *Quantum Mechanics and Path Integrals* (McGraw-Hill, New York, 1965).
 [20] R. I. Cukier *et al.*, *J. Chem. Phys.* **59**, 3873 (1973).
 [21] A. Saltelli, K. Chang, and E. Scott, *Sensitivity Analysis* (Wiley, New York, 2000).
 [22] S. A. Rice and M. Zhao, *Optimal Control of Molecular Dynamics* (Wiley, New York, 2000).
 [23] A. Bryson and Y. Ho, *Applied Optimal Control* (Hemisphere, New York, 1975).
 [24] C. Moler and C. V. Loan, *SIAM Rev.* **20**, 801 (1978).
 [25] For the four-level system $\mu_{12}=1.653$, $\mu_{13}=0.254$, $\mu_{14}=1.500$, $\mu_{23}=0.814$, $\mu_{24}=0.025$, $\mu_{34}=0.790$ (μ in 10^{-30} C m), $\omega_{12}=1.711$, $\omega_{13}=3.026$, $\omega_{14}=4.134$, $\omega_{23}=1.314$, $\omega_{24}=2.423$, $\omega_{34}=1.108$ (ω in rad/fs). The final time was $T=100$ fs.
 [26] For the seven-level system (only nonzero dipole moments are listed) $\mu_{12}=0.854$, $\mu_{13}=0.970$, $\mu_{24}=1.450$, $\mu_{34}=1.270$, $\mu_{45}=1.560$, $\mu_{46}=1.690$, $\mu_{57}=2.130$, $\mu_{67}=2.250$ (μ in 10^{-30} C m), $\omega_{12}=2.25$, $\omega_{13}=2.25$, $\omega_{14}=6.13$, $\omega_{15}=7.71$, $\omega_{16}=7.71$, $\omega_{17}=9.41$ (ω in rad/fs). The final time was $T=100$ fs.
 [27] Wilson Rugh, *Linear System Theory*, 2nd ed. (Prentice-Hall, Upper Saddle River, NJ, 1996).